

Solar irradiance in Gauteng during the 2020 COVID-19 lock-down – can we detect decreased aerosol loading?

Charles H Fourie¹, Hartmut Winkler¹ and Kittessa Roro²

¹ Department of Physics, University of Johannesburg, PO Box 524, 2006 Auckland Park, Johannesburg, South Africa

² Energy Centre, Council of Scientific and Industrial Research (CSIR), Building 34, Pretoria, South Africa

Corresponding author email: hwinkler@uj.ac.za

Abstract. This paper seeks to investigate the impact of aerosol loading in Tshwane (Pretoria) during the initial 35-day COVID-19 lock-down period in March-May 2020 using solar irradiance data obtained from pyranometer and spectroradiometer measurements. We seek to detect and identify possible aerosol loading reductions over that period due to lowered combustion and emissions associated with urban and industrial processes. Any such decline would manifest itself in a higher-than-average direct solar beam intensity and a lower incidence of scattered photons reaching the detector from different directions than the solar beam. We measure these irradiation components both spectroscopically and in integrated broadband form for selected days deemed free of cloud. We examine the relationship of the irradiance to the solar zenith angle, and confirm this to be well represented by a power law. A comparison of the 2020 results to similar determinations for selected days in 2018 and 2019 shows no difference between the seasonal averages, and we therefore conclude, in contrast to what would be expected in view of reduced anthropogenic activity, that the impact of the lockdown on aerosol levels was minimal.

1. Introduction

The Earth's atmosphere contains varying levels of suspended particles referred to as aerosols that by their presence reduce incoming solar radiation and decrease long distance visibility. This decreased transparency is also referred to as turbidity. While some aerosols are natural, many are also generated through human activity, which can lead to enhanced turbidity in urban areas [1].

During the early high-level lock-down linked to the COVID-19 pandemic in 2020, much of the South African industrial and economic sectors ground to a halt. The lower transport and industrial activity is well illustrated in human mobility data determined from communication device locations (see <https://www.google.com/covid19/mobility/>). This provided an opportunity to identify the role human activities have on the local contribution to aerosol emissions in Gauteng province, the most urbanized and industrialised region in South Africa, by comparing the 2020 atmospheric turbidity during that time of the year with the levels observed in prior years. This is done by measuring the solar beam strength during the lockdown months and comparing this to earlier periods.

The downscaling of activities lowers emissions due to industrial activity and transportation, but also leads to heightened domestic burning. The degree to which these processes affect aerosol concentration at a specific site furthermore depends on specific local meteorological conditions, especially wind.

2. Solar Irradiance

2.1. Solar Geometry

As the Earth orbits the Sun and the Earth rotates around its polar axis, the position of the Sun in the sky is constantly changing. As the angle of inclination of a solar beam reaching the surface changes, so does the amount of atmosphere a photon in the solar beam would pass through. The solar zenith angle (θ_z) is measured between the vertical and the incoming solar beam. This depends on the time of day, day of the year and latitude. Various procedures are available to calculate θ_z at any particular moment, the choice depending on the level of accuracy required (e.g. [2]). On any particular day, θ_z is at a minimum at solar noon, which is defined as the time when the Sun passes the meridian.

The parameter m , referred to as the airmass, equates to the amount of atmosphere a photon of light must pass through before reaching the ground. Its units are such that $m = 1$ corresponds to the vertical path from ground level to the top of the atmosphere. When ignoring distortions due to Earth curvature and refraction, airmass can be approximated by $m = \cos \theta_z$.

2.2. Radiation losses and light scattering in the atmosphere

Solar irradiance passing through the atmosphere may interact with some of its constituents, leading to a photon being absorbed or deflected into a different direction through scattering. The amount and spectral distribution of the radiation detected at ground level is influenced by numerous factors, such as the albedo (which refers to the reflected light from a surface), as well as the concentration of atmospheric gasses such as carbon dioxide, water vapour and other trace gases [3]. Different aerosols affect the spectrum of incoming solar radiation at different wavelengths. Factors determining this include particle size, as well as chemical or molecular composition, which determine energy states and the wavelengths of photons associated with atomic and molecular transitions. This results in scattering and absorption at specific wavelengths. The absorption bands for various aerosols and related radiation attenuation processes have been well documented (e.g. [4]).

2.3. Radiation components and spectral distribution

Global horizontal irradiance G is defined as the energy per unit time and per unit area collected by a horizontally placed detecting surface. There are two components contributing to this. The first is the solar beam, i.e. the sunlight reaching the surface that was not absorbed or scattered during the traverse of the atmosphere. We refer to this as the direct normal irradiance I . Given that the solar beam makes an angle of θ_z with the normal to the horizontal measuring surface, the effective detector surface area seen by the beam is reduced by a factor of $\cos \theta_z$. The second component contributing to G is the scattered radiation from the sky dome. This is referred to as the diffuse horizontal irradiance D . All these quantities are thus related to each other by the following expression:

$$G = I \cos \theta_z + D \quad (1)$$

While the accurate characterization of the global irradiance is extremely complex, there are mathematically very straightforward model formulations available that are able to approximate the actual relationship between G and θ_z quite well. One reasonably successful such formulation is a power law relationship sometimes referred to as the Adnot-Bourges-Campana-Gicquel clear-sky model (hereafter ABCG model) [5], defined by the following expression:

$$G = A(\cos \theta_z)^B \quad (2)$$

Note that the scaling parameter A corresponds to the global horizontal irradiance when the Sun is directly overhead (i.e. $\theta_z = 0 \Rightarrow \cos \theta_z = 1$). G will then be highest when radiation losses in the atmosphere are at their lowest, and hence A is an indicator of atmospheric transparency. This also applies to the majority of days when the Sun does not reach the point directly overhead at noon. The parameter B describes the deviation from a pure cosine form (which corresponds to $B = 1$). A value of $B \gg 1$ indicates enhanced irradiation when the Sun approaches the horizon, i.e. higher aerosol concentrations.

2.4. The Solar spectrum

Solar radiation is emitted by our Sun with a spectral form largely resembling a blackbody characteristic of its effective surface temperature of 5800 K. Most of the emitted sunlight is radiated in the near ultraviolet (0.28–0.40 μm ; UV), visible (0.40–0.70 μm) and infrared (0.70–3.0 μm) regions [6].

When studying the spectral properties of irradiance, it is useful to introduce another parameter, the spectral irradiance, which quantifies the irradiance per unit wavelength interval. In terms of the solar beam, this parameter is then referred to as the direct normal spectral irradiance I_λ , and is related to I by

$$I = \int_0^\infty I_\lambda d\lambda . \quad (3)$$

3. Methodology

We examine Council for Scientific and Industrial Research (CSIR) solar spectral irradiance, broadband irradiance and weather data for the period in question together with corresponding data from the two previous years. The broadband and weather data also form part of the regional Southern African Universities Radiometric Network (SAURAN) database [7].

We categorise days and months according to the measured degree of turbidity for the period April–July for 2018 and 2020 through analysis of the relationship between the measured irradiance and the solar zenith angle on cloud-free days. To eliminate the influence of cloud cover and other obstructions candidate clear-sky days were checked visually by inspecting the smoothness and morning-to-afternoon symmetry of the G vs. time plots for that day. We thus identified four days in 2018, six days in 2019 and seven days in 2020 which did not show signs of cloud interference. In the analysis later on we restrict ourselves to irradiance measurements taken when the solar zenith angle is smaller than $\theta_z = 84^\circ$, because, as with other simplistic models, the ABCG model fails when the Sun is close to the horizon.

The instrumentation used to secure the irradiance data was supplied by the CSIR, and is located on a rooftop on its main campus in Tshwane (Pretoria). The exact measurement site location is longitude 28.2787 E, latitude 25.7465 S and the altitude is 1400 m above sea level. The instruments were:

- Two pyranometers. When placed on a horizontal surface they directly measure G . The diffuse component D can also be determined with a pyranometer by obstructing the direct solar beam with a shading ball. The pyranometers we used are manufactured by Kipp & Zonen and are sensitive in the wavelength range 0.28–2.80 μm . They were set up to take measurements at a frequency of once every 30 seconds and record data every minute.
- A spectroradiometer manufactured by EKO-Weiser. It measures the direct normal spectral irradiance I_λ in the wavelength range 0.28–1.10 μm at 5 second intervals and recording data every minute.
- Weather data was gathered by a standard integrated weather sensor, which recorded wind data, temperatures, humidity and precipitation at 30 second intervals.

4. Results and analysis

4.1. Global horizontal irradiance model fits

This A and B parameters in the ABCG model are then obtained by linearising G as a function of $\cos \theta_z$ through the application of a logarithm to both sides of equation 2:

$$\log_{10} G = \log_{10} A + B \times \log_{10} (\cos \theta_z) . \quad (4)$$

Figure 1 illustrates one such plot. The best fitting line is determined by applying routine linear regression analysis, which then yields the parameters A and B . A comparison of the model for G and the actually measured data over the course of a day is shown in figure 2.

The R^2 values ranging between 0.988 and 0.999 highlight the high degree of linearity in the plots, not only confirming the suitability of the model, but also that the days chosen were indeed clear. Figure 3 is a plot of A vs. B , and there is no evidence of a systematic shift of the points for 2020 compared to the previous years.

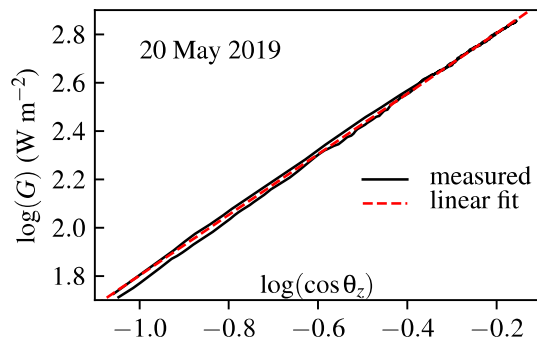


Figure 1. Example of a linearised $\log G$ vs. $\log(\cos \theta_z)$ plot.

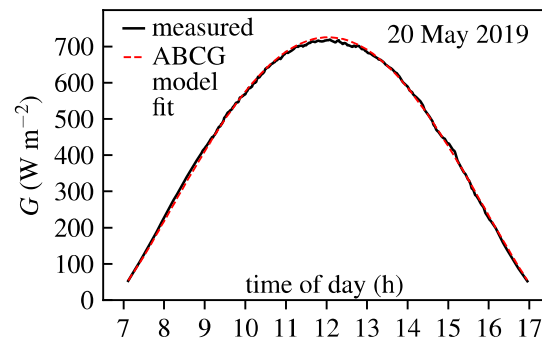


Figure 2. Comparison of the measured and model global horizontal irradiance values.

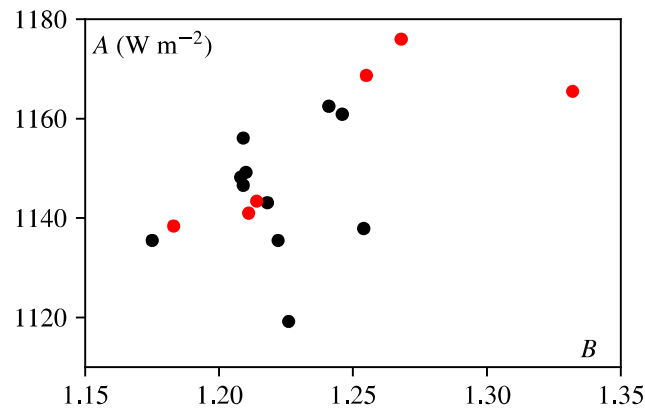


Figure 3. ABCG model A vs. B fitting parameters for selected clear days in 2018-2019 (in black) and in 2020 (in red).

The A and B fitting parameters are always higher than the values originally associated with the ABCG model. This can be attributed to differences in elevation and changed environment to the low altitude central European localities where the ABCG model was originally developed [5]. The RMSE values in table 1, were obtained by comparing the measured values of G to the values modelled using the ABCG formulation with A and B values obtained from fitting a straight line to the $\log G$ vs $\log(\cos \theta_z)$ plots analogous to the example shown in figure 2:

$$RMSE = \left(N^{-1} \sum (G(\text{model}) - G(\text{measured}))^2 \right)^{1/2}. \quad (5)$$

The number of values for each day varies as the ABCG model is restricted to $\theta_z < 84^\circ$, as measurements nearer to the horizon can be affected by shading through nearby buildings and trees. In addition to determining fitting parameters, the log-log plots can highlight variations in aerosol loading between morning and afternoon. The example shown in figure 1 is such a case.

The analysis performed in this section confirms that broadband values for 2018, 2019 and 2020 have not shown any clear evidence in a reduction in aerosol absorption, which would have resulted in an increase in the values of G and I with a corresponding decrease in D .

4.2. Solar noon irradiance comparison

As an alternative method of analysis, we compared the global horizontal, diffuse horizontal and direct normal irradiance at solar noon for the days investigated. G and D have been measured directly, while I can be calculated from these with equation 1.

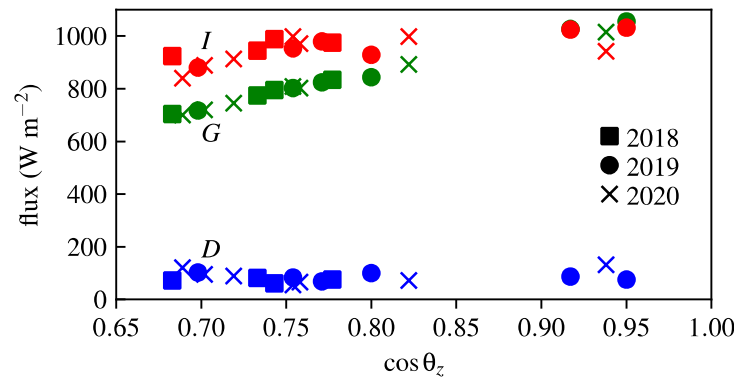


Figure 4. The measured values of G (in green) and D (in blue) at solar noon, and the corresponding values of I calculated from these using equation 1 (in red), plotted versus $\cos(\theta_z)$. The squares, circles and crosses represent the 2018, 2019 and 2020 data respectively.

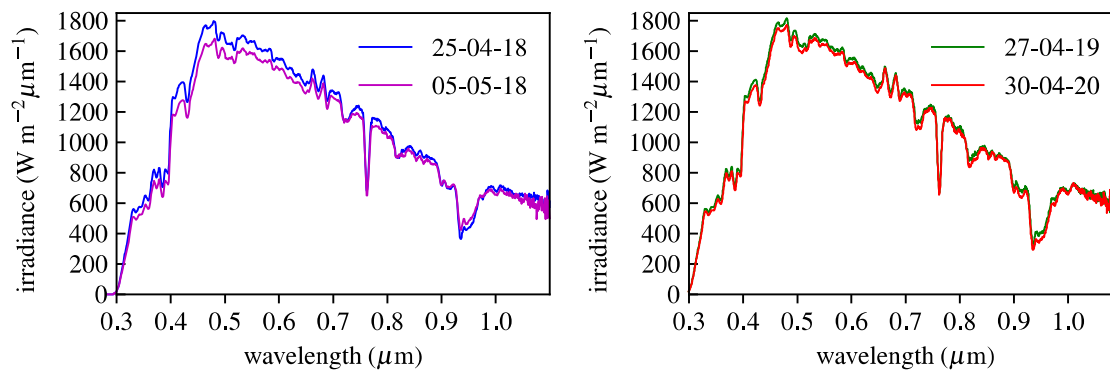


Figure 5. Spectral irradiance profiles for 2018-2020 (in $\text{W m}^{-2}\mu\text{m}^{-1}$).

Figure 4 compares the global, direct and diffuse irradiance at solar noon to the corresponding $\cos \theta_z$. The 2020 values of G and I would for a given θ_z be higher and for D be lower than those for the earlier years if the atmosphere was indeed clearer during the 2020 lockdown. There is no evidence for this. To demonstrate this, we fitted power law curves to the combined 2018-2020 data and determined the average offsets of the data points of the 2020 data. For 2020 we get: $\Delta G = -4.6 \pm 12.8 \text{ W/m}^2$, $\Delta D = +7.7 \pm 28.0 \text{ W/m}^2$ and $\Delta I = -11.6 \pm 51.1 \text{ W/m}^2$, meaning that the 2020 measurements are statistically consistent with the three-year average. If anything, there is a tendency for G and I to be lower and D to be higher in 2020, the opposite of what one would expect in the event of a clearer atmosphere.

4.3. Spectral Irradiance profile

Spectral profiles were inspected to identify possible variations in the absorption profiles in the 0.30-1.10 μm spectral range. The spectra were always taken close to solar noon, and within a week of 1 May so that the spectra all correspond to similar solar zenith angles.

All four spectral profiles in figure 5 show similar trends in spectral absorption bands for natural atmospheric aerosols. When looking at the UV region, clear signs of ozone absorption are visible, particularly in the UV spectrum, as well as the 0.45 μm to 0.75 μm region. Similarly, water vapour

absorption can be observed at 0.72 μm , 0.82 μm and 0.94 μm . Molecular oxygen exhibits absorption at 0.63, 0.69, 0.76 and 1.06 μm [3].

There is no obvious difference in the spectral shape between 2020 and the other years. The small variations between the displayed spectra can easily be explained as the result of the slow seasonal drift to larger airmass at solar noon, which leads to a slight weakening of I_{λ} as one moves towards mid-winter. There is also no sign of any changes to specific spectral lines. All this supports the earlier finding that the lockdown months of 2020 experienced normal aerosol loading.

5. Discussion

There are two ways to interpret the findings presented here: i) atmospheric particle concentrations at the measurement site have always been low even though this is an urban site; or ii) the methodology employed here and chosen sample are inadequate to detect changes in aerosol loading.

Looking at the first hypothesis, we note that the measurement site at the CSIR is comparatively removed from major industrial sites, so the downscaling of industrial operations during the COVID-19 lockdown would not have had a major impact there. Emissions from domestic coal fires would, if anything, have been more frequent during the lockdown due to more people being at home during the day. This could have counteracted the decrease in vehicle emissions. We also note that atmospheric transparency measurements carried out at the CSIR do not differ dramatically from those at some very remote locations [8], indicating that the CSIR site enjoyed only moderately aerosol loaded even in the pre-COVID lockdown period.

It is also possible that a larger number of daily data sets would have yielded a significant difference in sky transmission characteristics. For example, we note that the three days with the largest values of the ABCG model parameter A were all in 2020 (see figure 3). We also checked wind characteristics [9] on the days when our irradiance data was gathered, and found that there was wind with speeds of the order of 10 km h^{-1} on virtually all clear days chosen for 2018 and 2019. That would have assisted in dissipating locally polluted air on those days.

6. Conclusion

We attempted to detect whether the lockdown period at the start of the COVID-19 pandemic followed trends as seen in other major international cities of a significant decline in pollutants being emitted into the atmosphere. We find that, at least as far as average sky transparency is concerned, the urban region near our measurement site shows no evidence of lowered emission as a result of the March-May 2020 shut down of most economic and industrial activities.

References

- [1] Piketh S J, Annegarn H J and Tyson P D 1999 *Journal of Geophysical Research* **104** D1 1597
- [2] Blanco-Muriel M, Alarcon-Padilla D C, Lopez-Moratalla T and Lara-Coira M 2001 *Solar Energy* **70** 431
- [3] Patadia F, Levy R C and Mattoo S 2018 *Atmospheric Measurement Techniques* **11** 3205
- [4] Gueymard C A 2004 *Solar Energy* **76** 423
- [5] Badescu V 1997 *Solar Energy* **61** 251
- [6] Jacobson M Z 2013 *Fundamentals of Atmospheric Modelling* (Cambridge: Cambridge University Press) p 317
- [7] Brooks M J, du Clou S, van Niekerk J L, Gauche P, Leonard C, Mouzouris M J, Meyer A J, van der Westhuizen N, van Dyk E E and Vorster F 2015 *Journal of Energy in Southern Africa* **26** 2
- [8] Javu L, Winkler H and Roro K 2021 submitted to *Solar Energy*
- [9] <https://www.worldweatheronline.com>